Peer-reviewed version available at Actuators 2019, 8, 47; doi:10.3390/act8020047

Article

Compact and Powerful: A Vacuum Powered Soft Textile-Based Clutch

Ali Sadeghi[1,*], Alessio Mondini [1] and Barbara Mazzolai [1,*]

[1] Center for MicroBioRobotics; Istituto Italiano di Tecnologia (IIT); Pontedera (Pisa), 56025; Italy
* Correspondence: ali.sadeghi@iit.it; barbara.mazzolai@iit.it

Abstract: In this paper, we present the design, manufacturing and characterization of a soft textile-based clutch (TBC) that switches between locking and unlocking of its linear displacement by exploiting vacuum stimulation. The applied vacuum locks the relative sliding motion between two elaborated textile webbings covered by an elastic silicone rubber bag. Based on different fabrication techniques, such as silicone casting on textile, melt embossing for direct fabrication of miniature patterns on textile and sewing, we developed three groups of TBC samples based on friction and interlocking principles and we compared their performance in blocking configuration. The clutch with interlocking mechanism presented the highest withstanding force (150 N) respect to the one (54 N) recorded for the friction-based clutch. The simple and compact structure of the proposed clutch, together with the intrinsic adaptability of fabric with other clothing and soft materials, make it a proper solution for applications in soft wearable robotics and generally as locking and variable stiffness solution for soft robotic applications.

Keywords: soft clutch; soft robotics; textile based clutch; wearable robotics; soft actuator, exosuit; variable stiffness; stiffness control; textile

---

1. Introduction

Clutches are locking devices widely used in robotic systems. They switch between allowing and preventing relative motion of two parts mainly for energy management, reconfiguration, and safety reasons. In addition to conventional use of clutches for engaging and disengaging the driven components from the driving source , they are also used to lock and unlock robot motions and provide the capability of reconfiguration [1]. For example, in modular and reconfigurable robots, the use of clutches reduces the number of actuators and consequently results lighter weight modules [2,3]. Similarly, in underactuated systems, the use of clutches permits achieving high degrees of configurability with low number of actuators [4]. Moreover, the approach of using clutches as an essential component for decoupling from actuators and impedance control permits robots with rigid arms achieving softer and safer interactions with the environment [5].

In many robotic designs, clutches are powerful components for storing and fast releasing elastic energy for different aims, such as jumping in mobile [6,7] and legged robots [8]. Particularly, in unpowered and quasi-passive exoskeletons, clutches play a key role in storing elastic energy that permits force development with low or zero energy cost for assisting the wearer (e.g. patient) during walking [9-11].

Underactuated exoskeletons often integrate conventional rigid clutches for direct freezing and control of the wearer joints without the use of actuators, such as electromagnetic [12,13], electrostatic [11], magnetorheological fluid-based [14], or electrorheological fluid-based [15] clutches. In the recent years several promising examples of soft exosuits have tried to bring comfort and higher adaptability

Peer-reviewed version available at *Actuators* **2019**, *8*, 47; doi:10.3390/act8020047

to the wearer body by the use of intrinsically soft and light structural materials (e.g., textiles and soft elastomers) and soft actuation technologies [16]. Yet, most of the unpowered soft exosuits still include clutching systems that are mainly based on rigid, bulky and heavy conventional clutches [17]. An example of flexible clutch, based on electro-static force for quasi-passive ankle foot orthosis exoskeletons, is presented in [11]. Still, the need of rigid and planar connection plates at each end for guarantying the parallel gap between electrodes induces a certain level of rigidity; also, the use of high voltage for wearable devices can cause safety problems. To address these issues (i.e., wearability, comfort and safety), here we propose an entirely soft textile-based clutch actuated by vacuum sources with unconventional load capabilities.

The power of vacuum is extensively exploited in several soft robotic technologies for two main areas of applications: actuation [18-20] and variable stiffness solutions [21,22]. The successful use of vacuum in a granular jamming based universal gripper [21], has motivated many other researches in exploiting a similar approach to tune the stiffness in soft structures for a plethora of applications, such as medical [23], and adaptive grasping [24]. Variable stiffness sleeves based on the jamming mechanism of rubbery granules under vacuum are proposed in [22] for stiffening wearer body joints in a soft exoskeleton. Similarly, in the layer jamming mechanism, the vacuum power pushes the internal layers of a soft multi-layer structure together and converts it to a relatively stiff body. This clutch like solution is also exploited in different fields, such as medical [25] and wearable robotics [26-29]. Although both the granular and layer jamming mechanisms have demonstrated promising variation of stiffness for different soft robotic applications, increasing the final stiffness of a structure by playing only on the amount of granules or layers result in bulky and heavy structures with higher stiffness not only in the active but also in the passive mode.

In this work, we introduce the design and development of a new soft robotic component, which is a textile-based clutch (TBC) that exploits vacuum as activation solution. TBC is highly compliant, lightweight, compact and soft clutch realized with low cost components (i.e., textile, plastic, silicone). High softness and adaptability with wearable technologies, combined with easiness of integration with other materials commonly used in soft robotic structures (e.g., silicone elastomers), motivate the use of textile as base material for the realization of TBC. With the aim of improving the blocking capabilities of TBC, the surface of textile layers is elaborated by integrating miniature plastic structures able to create an interlocking action between them. A comparison with other solutions based on high friction materials (to improve the blocking force) is also performed, demonstrating the effectiveness of the proposed solution. Activation strategies were also proposed and analyzed to improve the response time of TBC.

2. Materials and Methods

2.1 Textile-Based Clutch

The soft TBC presented in this work is a bilayer elastic belt that we can block its elongation by applying negative pressure (vacuum). TBC comprises two elaborated inextensible textile - woven cotton - webbings, both in series with an elastic textile band. The two layers are connected together from their heads by an inverse arrangement. Specifically, the head of each inextensible textile is fixed to the head of the elastic band in the other series. Finally, the bilayer assembly of textile bands is packed inside a flat and air sealed elastic cover that permits the easy elongation of the device (Figure 1a). In the passive or disengaged mode (Figure 1b and 1c), the two TBC layers can freely slide in front of each other and consequently the TBC elongates with a minimum force that, based on Equation 1, depends to the elasticity of the cover, elastic bands and frictional interaction between layers. The application of a negative pressure inside the elastic cover activates the TBC (engaging mode) and creates a temporary adhesion between textile layers (Figure 1d). In this mode, the flexibility of the elastic cover permits that the external environmental pressure squeezes the cover and pushes the inextensible textile webbings toward each other and causes their temporary and strong adhesion (Figure 1d). The zone that the elaborated inextensible textile webbings face each other (called interfacing zone) (Figure 1b) plays a key role in the adhesion strength during the engaging mode. As presented in Equation 2 the magnitude of engaging force ($F_{engaing}$) is a function of the applied negative pressure (ΔP) and the device characteristics, such as the area occupied by the elastic bands A_{el}, area of interfacing zone A_{in}, the frictional coefficient between textile layer and elastic bands μ_{tex} and the effect of elaboration technique ($\mu_{elaboration}$).

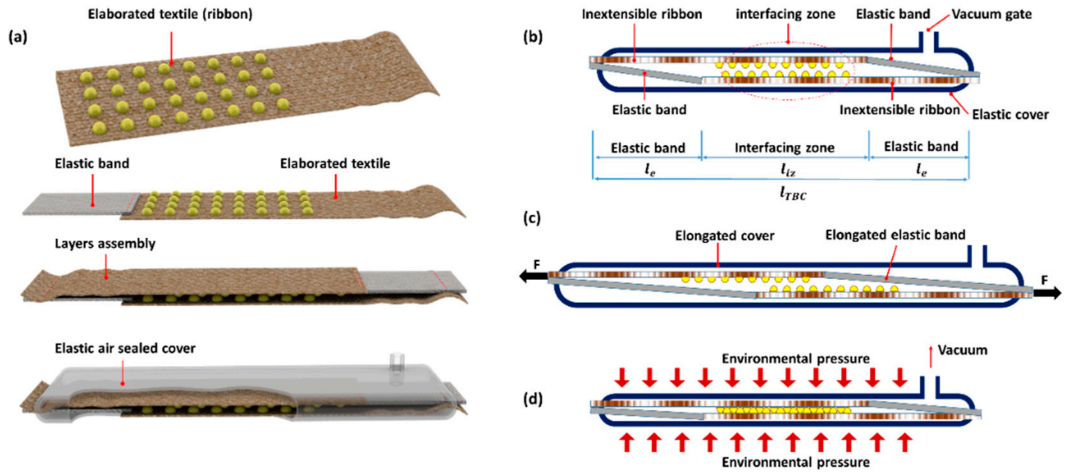

Figure 1. (a) CAD presentation of textile-based clutch TBC; two layers of textile parallel to each other are encapsulated inside an elastic cover. (b) and (c) Textile layers can slide in front of each other by means of an external elongation force; an elastic element in each layer of textile permits the device to elongate and recover its initial configuration. (d) Connecting the TBC to a vacuum source permits to the elaborated layers to create a temporary adhesion that blocks the elongation of the TBC under external elongation forces.

$$F_{elongation\ or\ dissengaing} = F_{elastics} + F_{internal\ friction}, \quad (1)$$

$$F_{engaing} = (\Delta P)\ (A_{el}\mu_{tex} + A_{in}\mu_{elaboration}), \quad (2)$$

The elongation ratio (ER_{TBC}) is an important parameter to characterize TBC and it is defined as the clutch elongation divided by the clutch length (l_{TBC}). According to the design in Figure 1b, l_{TBC} can be expressed as function of the length of interfacing zone (l_{iz}) and the length of elastic bands (l_e) (Equation 3). The maximum elongation is physically limited by the elongation ratio of the elastic bands (ER_e), but practically, for elongations greater than l_{iz}, the device cannot guarantee a proper engaging force and, in this situation, the interlocking of elaborated parts is not guaranteed. The ER_e and ER_{TBC} conditions that guarantee the TBC blocking for each elongation are defined in Equation 4. However, depending to the application of TBCs a longer elastic band can be selected where longer elongation range or lower elongation force during the disengaging mode is required.

$$l_{TBC} = l_{iz} + 2\ l_e, \quad (3)$$

$$ER_e < l_{iz}/l_e\ ,\ ER_{TBC} < l_{iz}/l_{TBC}, \quad (4)$$

A second characterizing parameter of TBC is the withstanding force in the engaged mode. This force can be modified by elaborating the frictional properties at interfacing zone. Utilizing materials with high coefficient of friction (e.g. rubber coating) on the surface of inextensible textile can enhance the TBC engaging performance without influencing the flexibility of the device. In this work, small and rigid segments (called bumps) integrated on the surface of inextensible textiles are used to permit a mechanical interlocking of the two textile layers to improve the withstanding force. This solution improves the clutching performance by adding the force of mechanical interlocking to the just frictional based force of engaging. Similar to the teeth in a dog clutch [30], the rigid bumps on each of the textile webbings can inter to the free space between bumps on the other webbing and cause an

Preprints (www.preprints.org) | NOT PEER-REVIEWED | Posted: 1 April 2019 doi:10.20944/preprints201904.0001.v1

Peer-reviewed version available at *Actuators* **2019**, *8*, 47; doi:10.3390/act8020047

interlocking action used for blocking the TBC elongation (Figure 1). Elaboration of the webbings by this technique does not interfere with their flexibility as the bumps are integrated in an array format (Figure 2a). This is because the area occupied by the rigid bumps in the array is small and the textile in the gap between the segments remains flexible (Figure 2b). Both geometry and frictional property of the bumps can influence the result of interlocking action during the engaging mode. In this work we selected a semispherical geometry for the bumps. During the disengage mode, bumps with semispherical shape easily slide on top of each other and do not significantly affect the elongation force. In the engaging mode (vacuum applied), each single bump is subjected to a normal force generated by the pressure and penetrates inside the front array of bumps, creating an engaging action that resists to the sliding of bumps on top of each other. In an array of semispherical interlocking bumps when all the bumps are penetrated inside each other the interlocking force can be obtained by Equation 5.

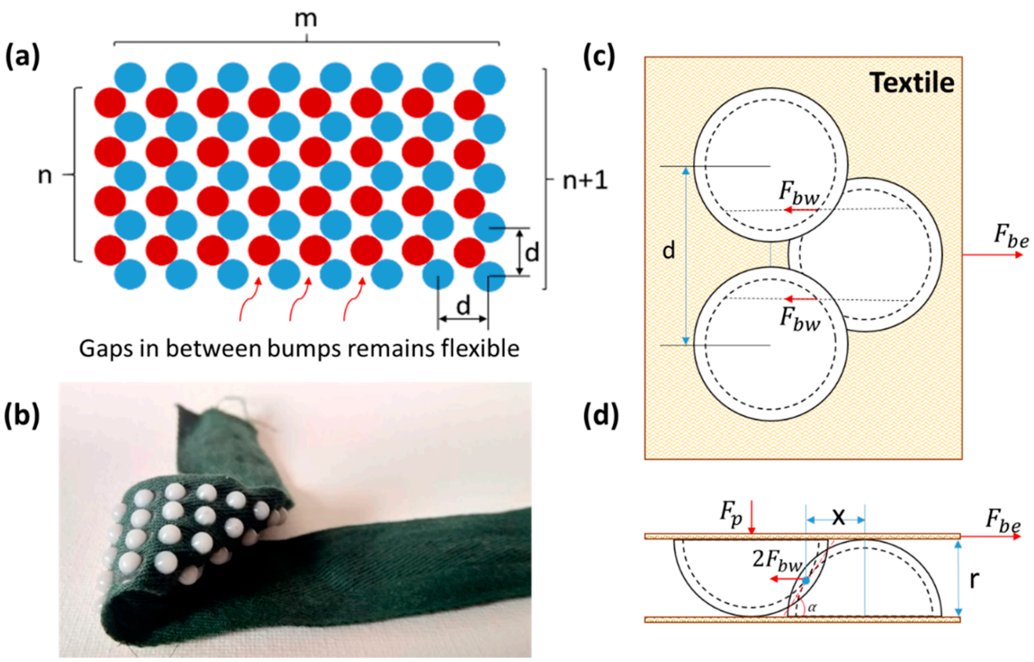

Figure 2. (a) The bumps of one layer (blue) inter to the gap between bumps of the front layer (red) and create an interlocking interaction. (b) A prototype of bumps array integrated on the surface of cotton webbing; the textile remains flexible after the bumps integration. (c) and (d) The top and side views of one bump interlocked with two bumps in the front layer; under force of environmental pressure F_p (generated by the vacuum), each bump can withstand the engaging force of F_{be} which is the sum of two forces F_{bw} acting on the bumps contacting points.

According Equation 5 and Equation 6, the size of bumps (r, the radius of semi-spheres), number of bumps in array (n×m), their distance (d) and their frictional properties (μ) can affect the withstanding force. Larger size of bumps can generate larger normal force caused by environmental pressure during the vacuum and consequently result bigger withstanding force, which is also influenced by the number of bumps as it is a sum of each bump engaging force (Figure 2). According to Equation 6 shorter is the distance d bigger is the engaging force. The x in this equation is the distance between the contact point of interlocked bumps and the center of each bump. Moreover, the distance of bumps should also satisfy the condition in Equation 7, otherwise no interlocking between bumps of two arrays is guaranteed. A tradeoff for the size of bumps is required, as the larger bumps can transform the environmental pressure to a higher normal force while smaller bumps permit to integrate higher number of bumps in a constant area of interfacing zone. The influence of size and density of bumps are investigated in our prototypes and experimental studies, which are reported in the next sections.

Preprints (www.preprints.org) | NOT PEER-REVIEWED | Posted: 1 April 2019 doi:10.20944/preprints201904.0001.v1

Peer-reviewed version available at *Actuators* **2019**, *8*, 47; doi:10.3390/act8020047

$$\mathrm{F}_{\mathrm{engaing}} = \Delta \mathrm{P} \left(\mathrm{A}_{\mathrm{elastics}} \mu_{\mathrm{ez}} + m \times n \times \pi r^2 \times 2F_p \times \frac{tan \propto + \mu}{1 - \mu \; tan \propto} \right), \quad (5)$$

$$tan \propto = \frac{2x}{r}, \quad x = \frac{\sqrt{12r^2 - d^2}}{4}, \quad (6)$$

$$d < 2\sqrt{3}\, r \quad (7)$$

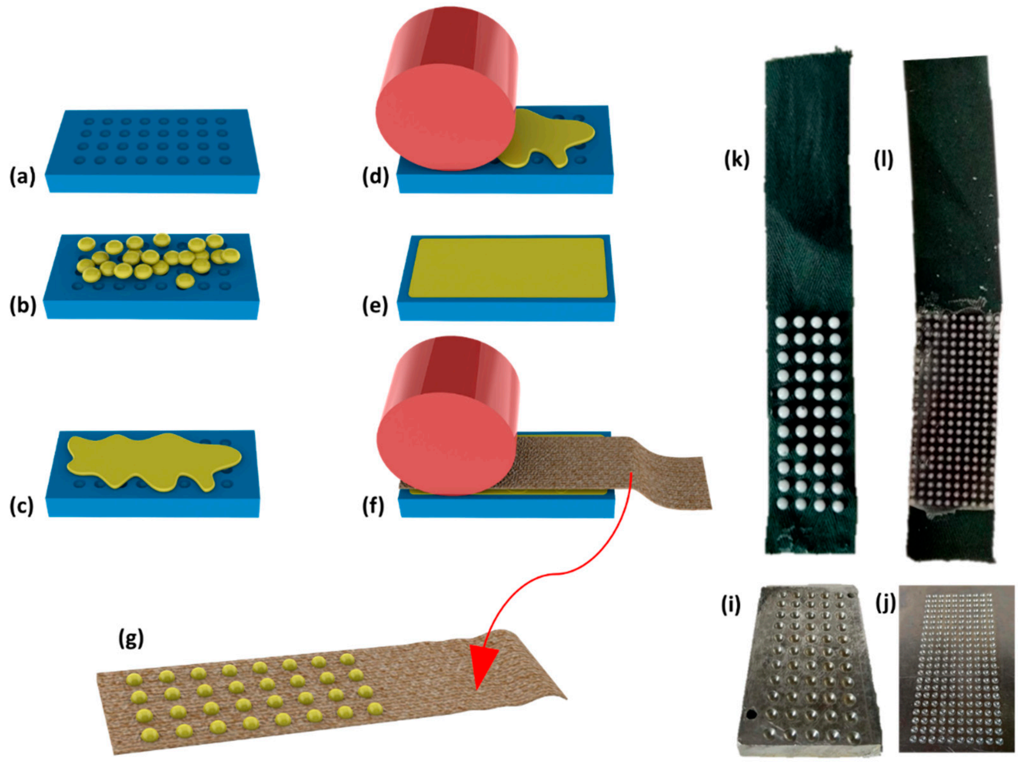

Figure 3. The process of bumps integration on textile: The metallic mold is pre heated (a) then the plastic pellets are added on it (b) and fused (c). After that, the fused material is pressed inside the mold by a roller (d) till a homogeneous flat surface is obtained (e). On that surface is then lie down the textile webbing (f) and the bumps are transferred on it (g). (k) Big bumps prototype. (i) Big bumps mold. (l) Small bumps prototype; (j) Small bumps mold.

2.2 Prototyping

We combined different techniques such as embossing, casting, and sewing to develop the TBC prototypes (Figure 3a to 3g). For each clutch, the arrays of rigid bumps were directly fabricated on a pair of woven cotton webbings (0.5 mm thickness and 30 mm width). Two series of TBC prototypes with semispherical bumps of 4 mm and 2 mm diameter were realized. The bumps were directly shaped and integrated on the textile webbings by CNC milled aluminum molds (Figure 3i and 3j). The metallic molds permit the fast and accurate realization of bumps array in one shot of pressing action. The granules of polyoxymethylen (POM) thermoplastic with high stiffness, and excellent dimensional stability [31], was firstly poured into the preheated (270°C) aluminum mold (Figure 3a and 3b). After fusing of granules, they were pressed inside the mold semispherical cavities by rolling a metallic cylinder over fused materials since a thin, flat and homogenous layer was obtained (Figure 3c to 3e and Supplementary Video1). The bumps inside the aluminum mold were transferred to the cotton webbing by locating the webbing on the top of the array and pressing it toward melted polymer, again by rolling of the metallic cylinder (Figure 3f). By pressing, the melted thermoplastic penetrates inside the textile porous texture and creates a strong bonding that is unified by the bump material. Finally, the assembly was removed from the mold after cooling the mold by cold water (Figure 3g). The strong bonding of bumps to the textile guarantees the stability of bumps in their

Preprints (www.preprints.org) | NOT PEER-REVIEWED | Posted: 1 April 2019 doi:10.20944/preprints201904.0001.v1

Peer-reviewed version available at Actuators 2019, 8, 47; doi:10.3390/act8020047

location under shear forces generated during the engaging action. TBCs with the 4 mm bumps integrate arrays of 5×11 bumps in front of 4×11 with 6 mm distance between bumps (Figure 3k); TBCs with 2 mm bumps were realized by arrays of 10×22 in front 9×22 with the distance of 3 mm in between bumps (Figure 3l). The webbings with one column less of bumps permit a symmetric configuration of webbings in the final assembly as the bumps of each webbing seats in the free space between bumps of the other webbing. An elastic textile band with 15 mm width and maximum 120% of elongation (Super-Elastic Prym Co.) was sewed to one head of each elaborated webbing. Sewing was selected as one of the best techniques that can adapt to the textile without affecting its properties or generating any rigidity in the connection point of elastic and non-elastic bands while providing a strong bonding. The total practical length of all the TBC prototypes was 180 mm while the length of interfacing area was 60 mm. For all the prototypes an elastic cover larger than the textiles assembly was realized by a casting process of silicone elastomer (Ecoflex 0030 of Smooth-On Co.) with a rectangular shape (50×220 mm, with 1 mm of wall thickness). Whole assembly of textile bands were inserted and sealed inside the elastic covers (Figure 4). A 4 mm silicone tube (SAINT-GOBAIN Co.) was later integrated to the elastic cover by silicone caulk.

Two other series of clutches based on just frictional materials were realized in order to compare the results with the TBC prototypes based on interlocking. Their interfacing zones were elaborated with high frictional coefficient materials: one by adhering sandpaper (P600) on the top and bottom sides of the interfacing zone; the second by coating 0.5 mm of silicone rubber at the interfacing zone which was achieved by direct sinking of textile webbing in silicone elastomer (Ecoflex 0030, Smooth-On, Inc.).

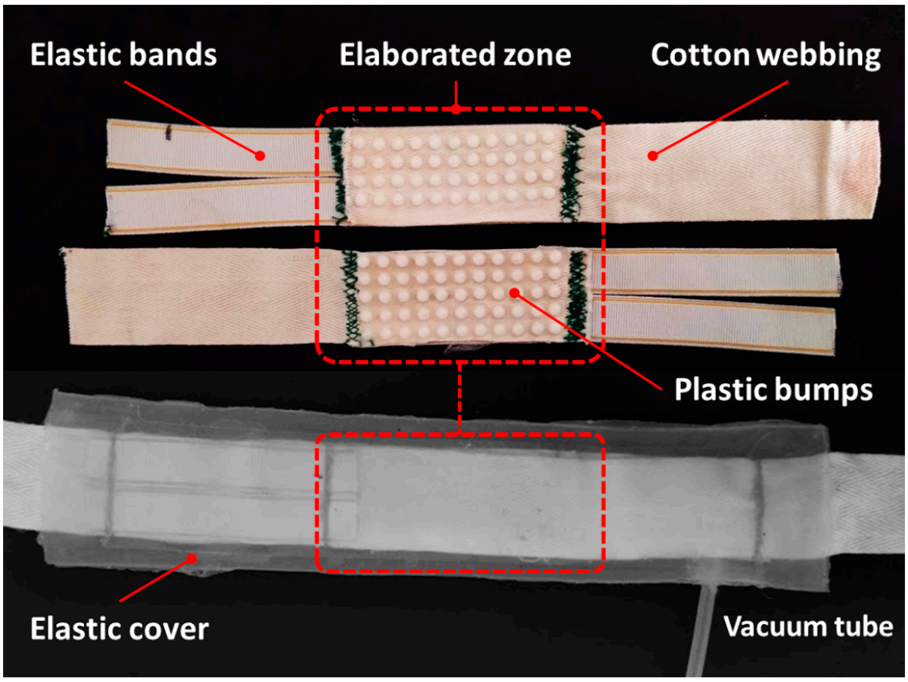

Figure 4. (top) The internal layers of TBC with elastic bands, elaborated zone with rigid bumps and inextensible cotton webbing; (bottom) Final assembled TBC inside the air sealed silicone rubber cover.

2.3 Clutch control unit

In order to address the requirements of compactness and mobility in wearable devices we developed a miniature pneumatic circuit that is managed by a custom control unit. A microcontroller (TMS320F28035 from Texas Instruments, Dallas, USA) regulates the pressure inside the TBC through two pneumatic valves (TX3P030LV03LN from First Sensor AG, Berlin, Germany) and a pressure sensor (MPXV6115V from NXP Semiconductor, Eindhoven, Netherlands). One of the two valves (Valve 1 in Figure 5) connects the clutch to the ambient pressure for the disengaging mode, while the other valve (Valve 2) connects the clutch to a vacuum chamber for the engaging mode. A second

Preprints (www.preprints.org) | NOT PEER-REVIEWED | Posted: 1 April 2019 doi:10.20944/preprints201904.0001.v1

Peer-reviewed version available at *Actuators* **2019**, *8*, 47; doi:10.3390/act8020047

pressure sensor is located between Valve2 and vacuum chamber to monitor the pressure of the chamber. A PC is connected to the setup by a serial interface (UART) to set the clutch pressure and acquire the pressure monitored by the system. A control loop is implemented in the microcontroller to keep the set pressure. Normally, both valves are deactivated; in this condition the clutch is closed and the pressure inside is kept to the reached value. We added a hysteresis of ±0.01 bar to the set value to avoid unnecessary valves activation and waste of energy. We used a vacuum chamber as vacuum reservoir that decouples the pump speed from the actuator speed. The vacuum chamber is brought to the desired vacuum level by the pumping system and then switched off. The developed system was used to characterize the clutch in terms of force and response time. In a real application, a constant pressure inside the reservoir can be guaranteed by the same control unit and by monitoring the pressure sensor between Valve 2 and reservoir.

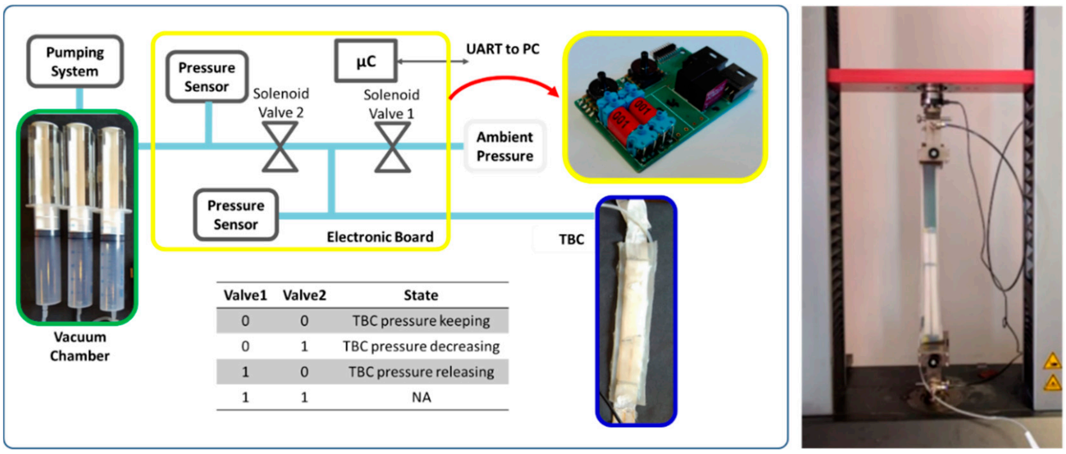

Figure 5. (left) Schematic of the control unit; two valves control the pressure inside the TBC. A chamber is used as vacuum reservoir and provides the possibility of several activation of TBC without direct use of vacuum pump; (right) Mechanical testing machine used to experimentally evaluate the TBC engaging force.

2.4 Experimental protocols and setups

Two sets of experiments were performed on the TBC prototypes to characterize their withstanding force under different conditions and their response time during engaging and disengaging actions. The force-elongation tests were performed by a material testing machine (Zwick/Roell Z005) and the pneumatic circuit discussed in the previous section to set the pressures in the TBCs (Figure 5 - right). We evaluated the engaging forces of all the TBC prototypes (friction based and interlocking based) under different negative pressures: 0 atm (no vacuum) to -0.8 atm with 0.2 atm steps, for 25 mm elongation with 100 mm/min linear velocity. The tests with no vacuum pressure (0 atm) were performed to measure the minimum force required for the elongation of TBCs in the disengaged mode. In order to clarify the frictional effect of the elaboration solutions on the minimum elongation force and separate it from the effect of elastic bands and the elastic covers, the elongation force of elastic cover and elastic bands were also separately characterized. The experiments were repeated for five times for three samples of each prototype. The response times of the interlocking TBC clutches for both engaging and disengaging actions can be affected by several aspects such as size of TBC clutches, volume and pressure level of the vacuum chamber, valves dimension, length and size of the pneumatic circuit and the desired final pressure level for the TBC. We evaluated the TBCs speeds with the same compact and portable control unit considering that one of the main applications of the clutch would be in soft exosuits where compactness, low weight and wearability are demanded. These measurements were made by evaluating the rate of pressure variation inside TBC during its activation. In order to investigate the influence of reservoir capacity on the response time of TBCs the experiments were repeated for three different sizes of vacuum reservoirs (50 ml, 100 ml and 150 ml) at maximum negative pressure (-0.8 atm). In these tests, when

Peer-reviewed version available at *Actuators* **2019**, *8*, 47; doi:10.3390/act8020047

the desired vacuum was achieved, the vacuum pump was disconnected from the chamber to exclude the performance of the pump from the reservoir effect. The disengaging response time were evaluated by connecting TBCs to a constant pressure of -0.8 atm (as maximum achieved negative pressure) and measuring the time needed to reach the ambient pressure one time Valve1 was open. To accelerate the response of TBCs with soft inflatable silicone covers, we hypothesized that pre-charging the device with a small negative pressure during the disengaging mode can reduce the device internal volume by deflating the cover and consequently reducing the engaging response time while the small negative pressure does not influence significantly the minimum elongation force in this mode. We experimentally evaluated this technique by applying small vacuum values while measuring the minimum elongation forces. Later based on this experiment, we evaluated the response time of TBCs when they were pre-charged by this negative pressure. All the experiments were repeated 5 times for each testing condition

3. Results & Discussion

In the tests at ambient pressure (0 atm) all the devices demonstrated a similar elongation force of 14.9 N, 15.7 N, 14.4 N, 15.1 N respectively for small bumps, large bumps, sand paper and silicone rubber coating. Comparing these measures with the elongation force of just the elastic bands together with elastic cover (14 N), we observed that large portion of elongation forces during disengaging mode is dedicated to the properties of elastic elements instead of the effect of frictional properties of elaborated techniques.

All the tested negative pressures were able to block the elongation of the interlocking TBC with different withstanding forces. As expected the highest maximum force was obtained with the TBCs elaborated by interlocking bumps. Both of the interlocking prototypes with small and large bumps presented better performance in comparison with friction-based TBCs (Figure 6 left). The average maximum withstanding force of small and large bumps interlocking TBCs were 150.5 N, 152.6 N, respectively, in correspondence of -0.8 atm for 25 mm elongation of TBC. In these prototypes the number of bumps ($m \times n$) multiplied for the area of each bump (πr^2) is almost the same. This justifies (equation 5) why we a big difference of withstanding force between them was not measured. The few differences of these measures would be due to the less conformability of silicone cover into the small gaps in between the small bumps, in comparison with the larger gaps in between the bigger bumps. The maximum measured forces for the TBC samples with sand paper and silicone coating were 138.7 N and 54.8 N under the same negative pressure (-0.8 atm).

At the beginning of each blocking test, we observed 12-15 mm extension of the textile webbings and therefore the first breaking of engaging action happened after that initial stretch of the textile. The force-displacement graphs of interlocking TBCs (Figure 6 middle and Figure 6 right) demonstrate the locking action of these type of clutches in the smallest vacuum pressure (-0.2 atm) and biggest vacuum pressure (-0.8 atm). The picks in these graphs relate to the moment that interlocking action of clutch fails and the bumps slide on top of each other and again seat inside the gap between them and the device recovers its locking action. For this reason, the distance between picks of the graphs corresponds the distance of bumps in the array of each prototype, which is 3 mm for the array with small bumps and 6 mm for the array with larger bumps. All TBCs, even after breaking the withstanding force, continue to elongate with an increasing force, which is due to the effect of elastic elements (elastic bands and elastic cover) as well as to an enlargement of the TBC area during elongation that results in a larger normal force generated by environmental pressure. Similarly, the proper action of the TBCs elaborated by sand paper was visible when the elongation of inextensible textile was stopped. This clutch, after its first breaking, demonstrated an engaging and disengaging behavior with very small picks in the force-displacement graph affected by miniature bumps of sand paper roughness. Differently, with the interlocking TBCs and sand paper the TBCs elaborated by silicone rubber without any clear breaking moment just demonstrated a growing force when the extension of the cotton webbing was finished. This clutch demonstrated a lower withstanding force with less sensitivity to the variation of pressure respect to other TBC prototypes but still the

Preprints (www.preprints.org) | NOT PEER-REVIEWED | Posted: 1 April 2019 doi:10.20944/preprints201904.0001.v1

Peer-reviewed version available at *Actuators* **2019**, *8*, 47; doi:10.3390/act8020047

maximum measured force was much higher than minimum measured force (disengaging mode) in ambient pressure.

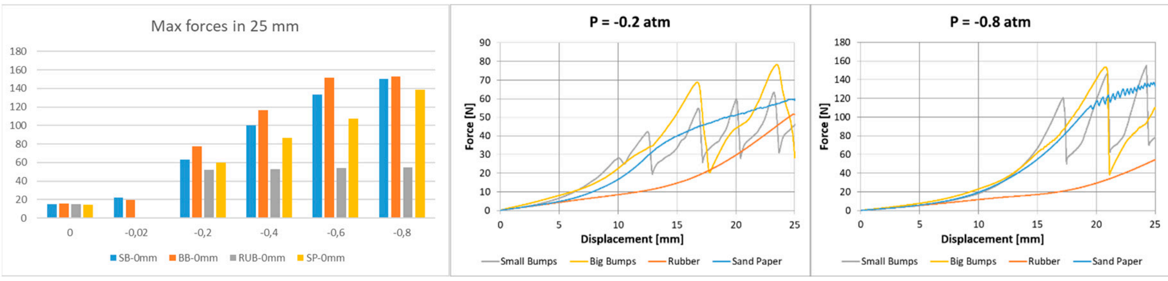

Figure 6. (Left): The mean maximum withstanding force of all the tested samples under different applied pressures (standard deviation ±1-3 N). (Middle) the force-displacement graph of all the TBCs under -0.2 atm and (right) under -0.8 vacuum pressure.

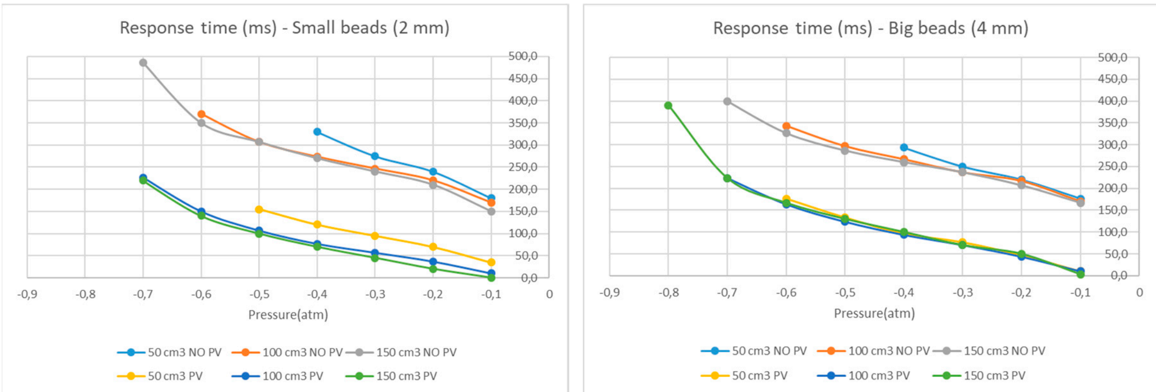

Figure 7. (left) the engaging response time of TBCs with small bumps; (right) the engaging response time of TBCs with large bumps (standard deviation ±3-8 ms). Both types of samples were tested in two different conditions; one starting from ambient pressure and one starting with a pre-charged pressure of -0.01 atm.

The results of the TBCs response time with small and rigid bumps and in engaging mode from environmental pressure to the different target pressures are depicted in (Figure 7 - left). We measured a slightly faster response time in the case of reservoirs with bigger volume. Also the TBC with bigger bumps was generally faster than the TBC with smaller bumps, probably because the elastic cover adapts easier in the large gap between large bumps (Figure 7 - right). The use bigger reservoirs allowed obtaining a better performance in achieving higher negative pressure inside TBCs. Therefore, in the case of applications that require high withstanding forces and consequently higher pressures, a bigger reservoir would be a good selection. We also recorded a faster response time in the experiments where TBCs were pre-vacuumed (internal pressure was set to -0.01 atm). The target pressure in the case of pre-vacuum was generally achieved 160 ms faster. For example, in the test with the slowest speed, TBC with large bumps took 350 ms to reach -0.6 atm while the same pressure was achieved in 160 ms in the case of pre-vacuum (190 ms faster). In general, the average response time of TBCs with small and large bumps respectively varies between 170-370 ms and 170-343ms in the normal case while by setting a pre-vacuum inside the clutches these range decrease to 3.3-226 ms and 10-223 ms for reaching -0.7 atm (with the chamber of 100 ml). This is while the elongation force does not show a significant difference between the -0.01 atm (19-20 N) and 0 atm (15-16 N) conditions. In addition to TBC performance, all of these results are also influenced by the performance of the fluidic system (e.g. valves, tubes, etc.)

Peer-reviewed version available at *Actuators* **2019**, *8*, 47; doi:10.3390/act8020047

About the disengaging mode, we recorded an average response time of 200 ms and 210 ms respectively for the TBCs with small and large bumps. The discharge response time also can become faster by blowing air inside the clutch, assisting the disengaging phase by a positive pressure.

4. Conclusions

In this work, we present a flat, compact and powerful soft clutching device that exploits intrinsic flexibility of textiles and silicone elastomers in its structural materials. The proposed component can simulate the functionality of conventional clutches and break in soft-bodied structure while it also has the capability of conformation and adaptation to different shapes. The textile-based clutches, i.e., TBCs, present a maximum withstanding force of 152 N, which is obtained using two layers of textile. TBCs also demonstrate a high withstanding-weight ratio of 340 times, considering the average weight of 45 g for all the developed prototypes. In addition to the interlocking TBCs, a series of friction-based clutches with coating of sand paper and silicone rubber were developed and characterized. The TBC elaborated by sand paper also demonstrated an acceptable performance with high withstanding force (average maximum of 138N), the practical issue with this type of TBC is the fast wear of sand paper under shear force and lose of performance after few cycle of use. Instead, the friction-based TBC developed by coating silicone on textile was the weakest TBC among other prototypes with maximum withstanding force of 54N. In contrast with interlocking TBCs, the silicone-coated TBC elongates smoothly with different forces under different applied negative pressures. Due to this behavior, the rubber-coated TBC can be potentially used as a variable stiffness elastic component with an elasticity that is tunable with pressure. The small size of TBCs results in a low internal volume that provides the possibility of achieving quite fast response time (in the order of 200 ms), even with a small and lightweight vacuum system. The high elongation ratio of the proposed device (up to 33 %) and the relatively fast response time of the clutches broaden its application in many different fields of application, such as wearable robotics. As example, the TBCs clutches can be integrated in a soft exosuit to limit and controlling the joints motions for assistive and rehabilitation applications [32]. In such application, the flat configuration and softness of developed clutch permit high adaptability to the wearer body and ease integration to textile based garments. Moreover, combination of this device in parallel or series with other elastic elements permits to engaging and disengaging or bypassing elastic elements in robotic structures that can have many applications in impedance control scenarios in legged robots and in unpowered exoskeletons and exosuits. The compact size of each TBC permits parallel configuration of several TBCs in a compact or flat assembly, which results greater withstanding forces for the case that loads higher than a single TBC is required. Moreover, as future work we aim to investigate the effect of different bump shapes and patterns on the performance of TBCs.

Supplementary Materials: The following are available online at www.mdpi.com/xxx/s1, Video S1: Clutch Fabrication, Video S2: TBC disengaged mode, Video S3: TBC weight lifting.

Author Contributions: "conceptualization, A.S.; methodology, A.S., A.M.; validation, A.S., A.M.; writing—original draft preparation, A.S.; writing—review and editing, A.S., A.M., B.M.

Funding: This work has received funding from the European Union's Horizon 2020 framework programme for research and innovation under grant agreement No 688175.

Conflicts of Interest: "The authors declare no conflict of interest." "The funders had no role in the design of the study; in the collection, analyses, or interpretation of data; in the writing of the manuscript, or in the decision to publish the results".

References

1. Plooij, M.; Mathijssen, G.; Cherelle, P.; Lefeber, D.; Vanderborght, B. Lock your robot: A review of locking devices in robotics. *IEEE Robotics & Automation Magazine* **2015**, *22*, 106-117.
2. Karbasi, H.; Huissoon, J.P.; Khajepour, A. Uni-drive modular robots: theory, design, and experiments. *Mechanism and Machine Theory* **2004**, *39*, 183-200.

Peer-reviewed version available at *Actuators* **2019**, *8*, 47; doi:10.3390/act8020047

3. Murata, S.; Kurokawa, H.; Yoshida, E.; Tomita, K.; Kokaji, S. A 3-D self-reconfigurable structure. In Proceedings of Robotics and Automation, 1998. Proceedings. 1998 IEEE International Conference on; pp. 432-439.
4. Aukes, D.M.; Heyneman, B.; Ulmen, J.; Stuart, H.; Cutkosky, M.R.; Kim, S.; Garcia, P.; Edsinger, A. Design and testing of a selectively compliant underactuated hand. *The International Journal of Robotics Research* **2014**, *33*, 721-735.
5. Lauzier, N.; Gosselin, C. Series clutch actuators for safe physical human-robot interaction. In Proceedings of Robotics and Automation (ICRA), 2011 IEEE International Conference on; pp. 5401-5406.
6. Armour, R.; Paskins, K.; Bowyer, A.; Vincent, J.; Megill, W. Jumping robots: a biomimetic solution to locomotion across rough terrain. *Bioinspiration & biomimetics* **2007**, *2*, S65.
7. Kim, K.-S.; Kim, B.-S.; Song, J.-B.; Yim, C.-H. Mobility improvement of a jumping robot using conical spring with variable length endtip. *Journal of Institute of Control, Robotics and Systems* **2009**, *15*, 1108-1114.
8. Zaitsev, V.; Gvirsman, O.; Hanan, U.B.; Weiss, A.; Ayali, A.; Kosa, G. A locust-inspired miniature jumping robot. *Bioinspiration & biomimetics* **2015**, *10*, 066012.
9. Collins, S.H.; Wiggin, M.B.; Sawicki, G.S. Reducing the energy cost of human walking using an unpowered exoskeleton. *Nature* **2015**, *522*, 212.
10. Walsh, C.J.; Endo, K.; Herr, H. A quasi-passive leg exoskeleton for load-carrying augmentation. *International Journal of Humanoid Robotics* **2007**, *4*, 487-506.
11. Diller, S.; Majidi, C.; Collins, S.H. A lightweight, low-power electroadhesive clutch and spring for exoskeleton actuation. In Proceedings of Robotics and Automation (ICRA), 2016 IEEE International Conference on; pp. 682-689.
12. Yakimovich, T.; Kofman, J.; Lemaire, E.D. Design and evaluation of a stance-control knee-ankle-foot orthosis knee joint. *IEEE Transactions on neural systems and rehabilitation engineering* **2006**, *14*, 361-369.
13. Muhammad, I.; AO, N.A. Stance-Control-Orthoses with Electromechanical Actuation Mechanism: Usefulness, Design Analysis and Directions to Overcome Challenges. *Journal of Neurology and Neuroscience* **2015**, *6*.
14. Chen, J.; Liao, W.-H. A leg exoskeleton utilizing a magnetorheological actuator. In Proceedings of Robotics and Biomimetics, 2006. ROBIO'06. IEEE International Conference on; pp. 824-829.
15. Nikitczuk, J.; Weinberg, B.; Canavan, P.K.; Mavroidis, C. Active knee rehabilitation orthotic device with variable damping characteristics implemented via an electrorheological fluid. *IEEE/ASME Transactions on Mechatronics* **2010**, *15*, 952-960.
16. Asbeck, A.T.; De Rossi, S.M.; Holt, K.G.; Walsh, C.J. A biologically inspired soft exosuit for walking assistance. *The International Journal of Robotics Research* **2015**, *34*, 744-762.
17. Poliero, T. Soft wearable device for lower limb assistance: assemsment of an optimized energy efficient actuation prototype. *Soft Robotics 2018, Livorno* **2018**.
18. Robertson, M.A.; Paik, J. New soft robots really suck: Vacuum-powered systems empower diverse capabilities. *Sci. Robot.* **2017**, *2*, eaan6357.
19. Yang, D.; Verma, M.S.; Lossner, E.; Stothers, D.; Whitesides, G.M. Negative - Pressure Soft Linear Actuator with a Mechanical Advantage. *Advanced Materials Technologies* **2017**, *2*.
20. Li, S.; Vogt, D.M.; Rus, D.; Wood, R.J. Fluid-driven origami-inspired artificial muscles. *Proceedings of the National Academy of Sciences* **2017**, 201713450.
21. Brown, E.; Rodenberg, N.; Amend, J.; Mozeika, A.; Steltz, E.; Zakin, M.R.; Lipson, H.; Jaeger, H.M. Universal robotic gripper based on the jamming of granular material. *Proceedings of the National Academy of Sciences* **2010**, *107*, 18809-18814.
22. Hauser, S.; Robertson, M.; Ijspeert, A.; Paik, J. Jammjoint: A variable stiffness device based on granular jamming for wearable joint support. *IEEE Robotics and Automation Letters* **2017**, *2*, 849-855.
23. Ranzani, T.; Gerboni, G.; Cianchetti, M.; Menciassi, A. A bioinspired soft manipulator for minimally invasive surgery. *Bioinspiration & biomimetics* **2015**, *10*, 035008.
24. Wei, Y.; Chen, Y.; Ren, T.; Chen, Q.; Yan, C.; Yang, Y.; Li, Y. A novel, variable stiffness robotic gripper based on integrated soft actuating and particle jamming. *Soft Robotics* **2016**, *3*, 134-143.
25. Kim, Y.-J.; Cheng, S.; Kim, S.; Iagnemma, K. A novel layer jamming mechanism with tunable stiffness capability for minimally invasive surgery. *IEEE Transactions on Robotics* **2013**, *29*, 1031-1042.
26. Bureau, M.; Keller, T.; Perry, J.; Velik, R.; Veneman, J.F. Variable stiffness structure for limb attachment. In Proceedings of Rehabilitation Robotics (ICORR), 2011 IEEE International Conference on; pp. 1-4.
27. Choi, I.; Corson, N.; Peiros, L.; Hawkes, E.W.; Keller, S.; Follmer, S. A Soft, Controllable, High Force Density Linear Brake Utilizing Layer Jamming. *IEEE Robotics and Automation Letters* **2018**, *3*, 450-457.

Peer-reviewed version available at *Actuators* **2019**, *8*, 47; doi:10.3390/act8020047

28. Sadeghi, A.; Mondini, A.; Mazzolai, B. Preliminary Experimental Study on Variable Stiffness Structures Based on Textile Jamming for Wearable Robotics. In Proceedings of International Symposium on Wearable Robotics; pp. 49-52.
29. Tonazzini, A.; Shintake, J.; Rognon, C.; Ramachandran, V.; Mintchev, S.; Floreano, D. Variable stiffness strip with strain sensing for wearable robotics. In Proceedings of 2018 IEEE International Conference on Soft Robotics (RoboSoft); pp. 485-490.
30. MASc, T.Y.; Jonathan Kofman PhD, P. Engineering design review of stance-control knee-ankle-foot orthoses. *Journal of rehabilitation research and development* **2009**, *46*, 257.
31. Visakh, P.; Chandran, S. *Polyoxymethylene Handbook: Structure, Properties, Applications and Their Nanocomposites*; John Wiley & Sons: 2014.
32. Ortiz, J.; Rocon, E.; Power, V.; de Eyto, A.; O'Sullivan, L.; Wirz, M.; Bauer, C.; Schülein, S.; Stadler, K.S.; Mazzolai, B. Xosoft-a vision for a soft modular lower limb exoskeleton. In *Wearable Robotics: Challenges and Trends*, Springer: 2017; pp. 83-88.